

π -Conjugation Enables Ultra-High Rate Capabilities and Cycling Stabilities in Phenothiazine Copolymers as Cathode-Active Battery Materials

Pascal Acker, Luisa Rzesny, Cleber F. N. Marchiori, C. Moyses Araujo, and Birgit Esser*

In recent years, organic battery cathode materials have emerged as an attractive alternative to metal oxide-based cathodes. Organic redox polymers that can be reversibly oxidized are particularly promising. A drawback, however, often is their limited cycling stability and rate performance in a high voltage range of more than 3.4 V versus Li/Li⁺. Herein, a conjugated copolymer design with phenothiazine as a redox-active group and a bithiophene co-monomer is presented, enabling ultra-high rate capability and cycling stability. After 30 000 cycles at a 100C rate, >97% of the initial capacity is retained. The composite electrodes feature defined discharge potentials at 3.6 V versus Li/Li⁺ due to the presence of separated phenothiazine redox centers. The semiconducting nature of the polymer allows for fast charge transport in the composite electrode at a high mass loading of 60 wt%. A comparison with three structurally related polymers demonstrates that changing the size, amount, or nature of the side groups leads to a reduced cell performance. This conjugated copolymer design can be used in the development of advanced redox polymers for batteries.

cathode materials^[15–18] with reported cell voltages of up to 4.1 V versus lithium as anode.^[19] Mainly, two classes of polymers have been considered, as shown in **Figure 1**: aliphatic redox polymers and conducting polymers. In the former, redox-active groups are covalently attached to an aliphatic polymer backbone, which serves to ensure their insolubility in battery electrolytes.^[4,17,18] Typical examples are polymers containing stable nitroxyl radicals in the side group.^[20–22] These polymers are usually electronically insulating, and charge transport between redox-active side groups can only occur through hopping processes or self-exchange between redox centers, which limits their rate capability. An advantage of these polymers is that they feature a stable redox potential, regardless of the charging state of the battery.


Conducting polymers, on the other hand, possess intrinsic conductivity in

1. Introduction

Organic cathode materials have been identified as promising candidates for next-generation battery systems.^[1–12] Their advantages include a high structural diversity and design flexibility as well as a low toxicity. In addition, they are accessible from less-limited resources compared to their inorganic counterparts.^[13,14] Redox polymers are among the best organic

the doped state, but sloping charge/discharge potentials due to the extensive delocalization of charges. Furthermore, often times only low doping levels are accessible in a reversible fashion.^[4,15,23,24] We herein present a combination of the benefits of both designs by using π -conjugated redox polymers **P1** and **P2** as cathode-active materials in a lithium organic battery (**Figure 1**). The resulting polymer-based composite electrodes of **P1a** and **P2** possessed both stable charge/discharge

P. Acker, L. Rzesny, Prof. B. Esser
Institute for Organic Chemistry
University of Freiburg
Albertstraße 21, 79104 Freiburg, Germany
E-mail: besser@oc.uni-freiburg.de
Prof. B. Esser
Freiburg Materials Research Center
University of Freiburg
Stefan-Meier-Str. 21, 79104 Freiburg, Germany

 The ORCID identification number(s) for the author(s) of this article can be found under <https://doi.org/10.1002/adfm.201906436>.

© 2019 The Authors. Published by WILEY-VCH Verlag GmbH & Co. KGaA, Weinheim. This is an open access article under the terms of the Creative Commons Attribution License, which permits use, distribution and reproduction in any medium, provided the original work is properly cited.

Prof. B. Esser
Cluster of Excellence livMatS @ FIT—Freiburg Center
for Interactive Materials and Bioinspired Technologies
University of Freiburg
Georges-Köhler-Allee 105, 79110 Freiburg, Germany
Dr. C. F. N. Marchiori, Prof. C. M. Araujo
Materials Theory Division
Department of Physics and Astronomy
Uppsala University
Box 516, 75120 Uppsala, Sweden
Dr. C. F. N. Marchiori
Department of Chemistry—Ångström Laboratory
Uppsala University
Box 538, 75121 Uppsala, Sweden

DOI: 10.1002/adfm.201906436

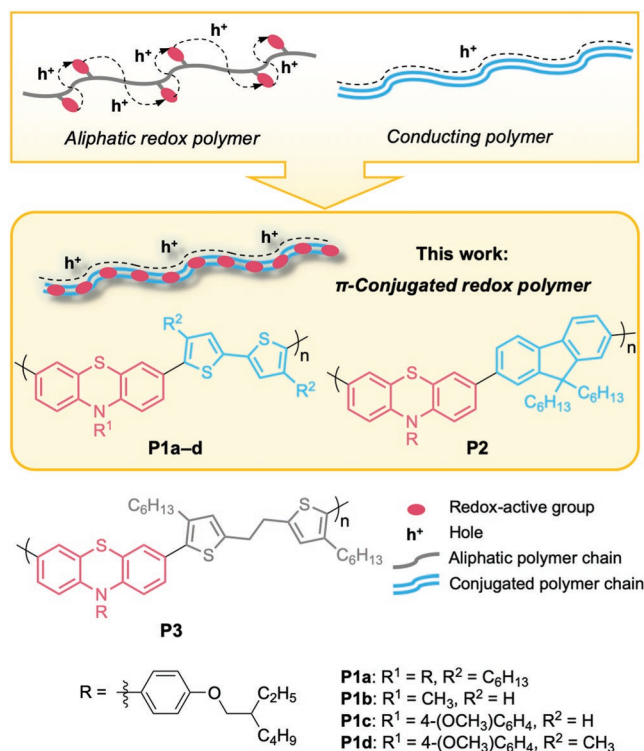


Figure 1. Combining defined redox centers, as present in aliphatic redox polymers, with a conjugated polymer backbone leads to π -conjugated redox polymers **P1a–d** and **P2** with well-defined oxidation potentials and hole transport along the polymer backbone. **P3** with broken conjugation served for comparison.

potentials due to the well-defined phenothiazine redox centers as well as ultra-high rate capability, and long-term cycling stability at 100C rate in the case of **P1a**, because of the semiconducting nature of the polymers. With 3.6 V versus Li/Li^+ , the discharge potentials in composite electrodes lay close to the operation potential of commercial Li-ion battery cathodes.^[25] In addition, they contained a high mass-loading of 60 wt% active material. **P1b–d** served to elucidate the influence of side chains on the battery performance of the polymers, and **P3** was used to assess the influence of π -conjugation (Figure 1).

The concept of a π -conjugated redox polymer as battery electrode material has been demonstrated before using the well-known n-type NDI-bithiophene copolymer P(NDI2OD-T2) with a discharge potential of about 2.4 V versus Li/Li^+ ,^[26] as well as the corresponding fluorene copolymer.^[27] In this work, a p-type conjugated polymer with phenothiazine was chosen based on its reversible oxidation chemistry, high oxidation potential of 3.6 V versus Li/Li^+ , and excellent performance in battery cathode materials.^[28–33] We recently demonstrated high cycling stabilities at 10C rate using poly(3-vinyl-N-methyl-phenothiazine) due to supramolecular hole-transport.^[28,29,34] In order to separate the redox-active phenothiazine moieties and to allow for good hole conductivity, we used bithiophene and fluorene as comonomers in **P1** and **P2**, respectively. An aryl ether group was chosen as substituent *R* to obtain highly reversible oxidation processes of the phenothiazine group upon oxidation,^[35] and alkyl

groups were attached in **P1a**, **P2**, and **P3** to ensure solubility of the polymers for purification and preparation of composite electrodes. Conjugated copolymers of phenothiazine with fluorene and bithiophene have been reported before for use in organic light-emitting diodes or photovoltaic cells,^[36–41] but not for battery applications.

2. Results and Discussion

2.1. Comparison of Bithiophene and Fluorene Copolymers and Influence of Conjugation

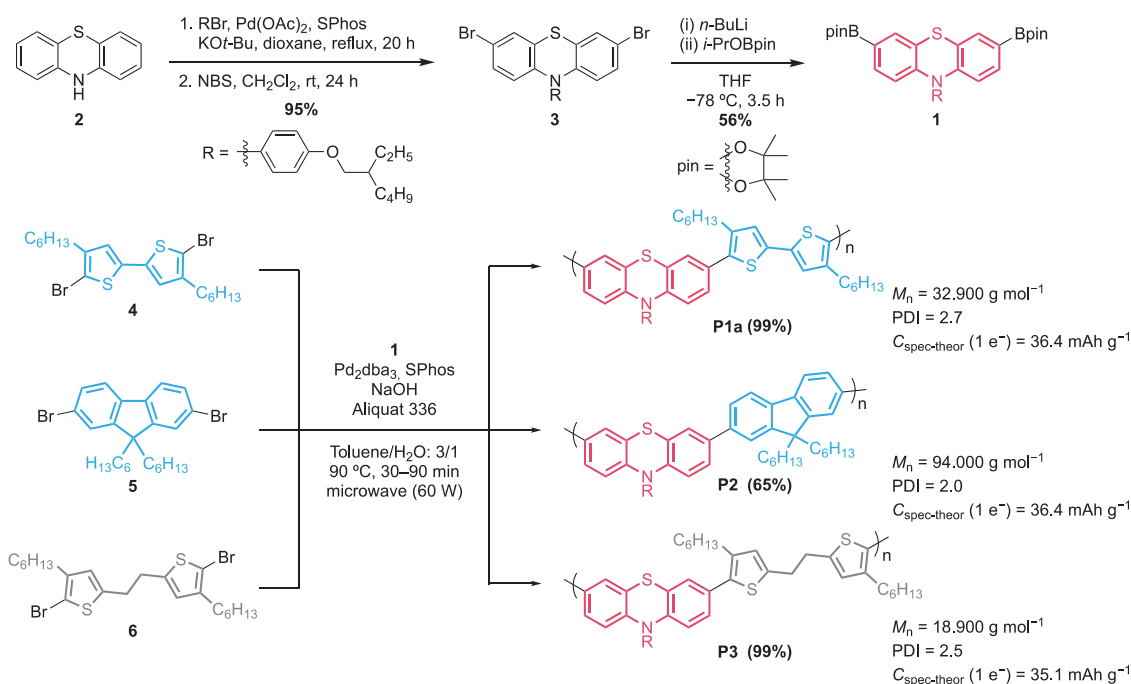
2.1.1. Synthesis of Polymers **P1a**, **P2**, and **P3**

The required phenothiazine monomer **1** was synthesized in three steps starting from phenothiazine (**2**, Scheme 1). Buchwald–Hartwig reaction allowed introducing the aryl ether moiety on the nitrogen atom, followed by twofold bromination to yield **3**. The bromo substituents were then replaced by boronic ester moieties to obtain **1**. Suzuki–Miyaura polycondensations of phenothiazine monomer **1** with the corresponding dibromides **4–6** yielded polymers **P1a**, **P2**, and **P3**, respectively (Scheme 1). **4**^[42] and **5**^[43] were synthesized according to the literature, and the synthesis of **6** can be found in Supporting Information. In order to obtain **P1–P3** with high molecular weights and in high yields, we performed an extensive optimization of reaction conditions, in particular concerning the catalyst and reaction mode (see Supporting Information for details). High molecular weights are important to ensure insolubility of the polymers in the battery electrolyte. Tris(dibenzylideneacetone)dipalladium with the ligand SPhos and sodium hydroxide as base in toluene/water (3/1) with Aliquat 336 as phase-transfer catalyst was the method of choice. We furthermore found that polymerization in a microwave synthesizer using SPS mode provided superior results and shorter reaction times compared to oil bath heating.

We assessed the thermal stability of **P1a**, **P2**, and **P3** using thermal gravimetric analyses. All three polymers possessed high decomposition temperatures above 405 °C (**P1a**), 402 °C (**P2**), and 402 °C (**P3**) (onset of decomposition in air, see Figures S59 and S60, Supporting Information).

2.1.2. Electrochemical and Optical Properties of Polymers **P1a**, **P2**, and **P3**

Cyclic voltammetry (CV) measurements and UV–vis absorption and emission spectroscopy provided information about the electrochemical and optical properties of **P1a**, **P2**, and **P3**, as summarized in Table 1. In solution, **P1a**, **P2**, and **P3** featured reversible oxidations at half-wave potentials of 0.20, 0.23, and 0.13 V versus Fc/Fc^+ , respectively (see Figure 2a–c). The second oxidations of the phenothiazine units in **P1a**, **P2**, and **P3** occurred at 0.77, 0.90, and 0.69 V versus Fc/Fc^+ , respectively (see Figure S45, Supporting Information). **P1a** showed two further oxidation waves at potentials of 0.69 and 0.92 V versus Fc/Fc^+ , likely because of the bithiophene units.



Scheme 1. Synthesis of polymers **P1a**, **P2**, and **P3** and theoretical specific capacities.

The absorption spectra of **P1a**, **P2**, and **P3** (see Supporting Information) displayed two main bands with maxima between 307 and 410 nm (Table 1). The optical band gaps lay between 2.44 and 2.66 eV. All three polymers were fluorescent with emission maxima of 519, 483, and 474 nm for **P1a**, **P2**, and **P3**, respectively (see Table 1 and Figure S56, Supporting Information).

2.1.3. Electrochemical Testing of Polymers **P1a**, **P2**, and **P3** as Cathode-Active Battery Materials

For the investigation of **P1a**, **P2**, and **P3** as cathode-active materials in batteries, we fabricated composite electrodes containing a high ratio of 60 wt% polymer, 35 wt% Super C65 as conductive additive, and 5 wt% PVdF binder. Metallic lithium was used as the counter and reference electrode and 1 M LiPF₆ in EC:DMC 1:1 as electrolyte. Scanning electron microscopic (SEM) measurements showed that the porous, percolated network structure of the carbon black Super C65 was maintained in the composite electrodes. The surface of the carbon network was evenly coated with the polymers, as confirmed by energy-dispersive X-ray spectroscopy (EDS) measurements (see Figures S62–S70, Supporting

Information, for SEM and EDS images). As seen from the CVs (Figure 2d,e), the oxidations of **P1a**, **P2**, and **P3** in composite electrodes occurred at potentials of 3.68, 3.70, and 3.59 V versus Li/Li⁺, respectively, around 0.2 V higher than would be expected from the values in solution (assuming 3.25 V^[45] for Fc/Fc⁺ versus Li/Li⁺). For **P1a** and **P2**, the oxidation peaks were narrow, indicating well-defined, faradaic redox processes, while **P3** showed broader peaks. This stands in contrast to polymers solely containing phenothiazine units with broad oxidation peaks.^[31,46,47] At 3.9/4.0 V versus Li/Li⁺, the second oxidations started setting in, visible in the cathodic scans (see Figure S45, Supporting Information).

Constant current cycling measurements at 1C rate (Figure 3a–d) in the range of 3.2–3.9 V versus Li/Li⁺ showed stable cycling behavior. All three polymers reached a value close to their theoretical capacity for one oxidation of each subunit, which amount to 36.4 mAh g⁻¹ for **P1a** and **P2** and 35.1 mAh g⁻¹ for **P3** (see also Scheme 1).^[48] After 100 cycles, capacities of 34.7, 33.4, and 31.0 mAh g⁻¹ were obtained for **P1a**, **P2**, and **P3**, respectively. For **P1a**, no loss in capacity was measured, while for **P2** the capacity had dropped by only 2%, demonstrating the high cycling stability of both polymers. The coulombic efficiencies lay between 97.6% and 99.6% (after cycle ten). The

Table 1. Electrochemical and optical data for **P1a**, **P2**, and **P3** in solution and in composite electrodes.

	<i>E</i> _{1/2} [V] ^{a)}	<i>E</i> _{1/2} [V] ^{b)}	<i>E</i> _{HOMO} [eV] ^{c)}	$\lambda_{\text{max,abs}}$ [nm] ^{d)}	$\lambda_{\text{max,em}}$ [nm] ^{d)}	<i>E</i> _{g,opt} [eV] ^{e)}
P1a	0.20	3.68	-4.88	354/410	519	2.44
P2	0.23	3.70	-4.94	329/398	483	2.59
P3	0.13	3.59	-4.81	307/398	474	2.66

^{a)}In CH₂Cl₂, internally referenced to the Fc/Fc⁺ redox couple; ^{b)}In composite electrodes versus Li/Li⁺; ^{c)}From the onsets of the oxidation peaks in solution, assuming an ionization energy of 4.8 eV for ferrocene^[44]; ^{d)}In CH₂Cl₂; ^{e)}Optical band gap from the onset of the longest wavelength absorption band.

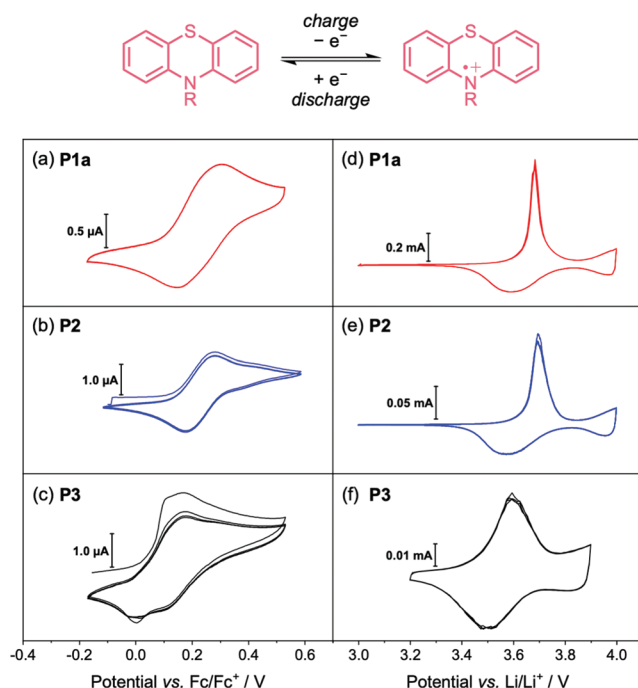


Figure 2. Reversible oxidation of phenothiazine to a radical cation and cyclic voltammograms of **P1a**, **P2**, and **P3** in solution (a–c) (100 mV s^{-1} , 1 mM in CH_2Cl_2 , 0.1 M $n\text{-Bu}_4\text{NPF}_6$, glassy carbon working electrode) and in composite electrodes (d–f) (0.2 mV s^{-1} , polymer/carbon black/PVdF [60:35:5 wt%], 1 M LiPF_6 in EC/DMC [1:1], counter/reference electrode: Li foil), four cycles each.

charge/discharge curves (Figure 3a–c) possessed flat plateau potentials for all three polymers at discharge potentials of 3.6 V for **P1a** and **P2** and 3.4 V for **P3** (all vs Li/Li^+). This shows that the phenothiazine units in all three polymers, even in conjugated **P1a** and **P2**, acted electrochemically separated, and that the oxidation potentials of the polymers were not affected by the charging state of the battery. This is a clear advantage in comparison to π -conjugated polymers, where usually sloping potential curves are obtained.^[4,23] The self-discharge, measured for **P1a**-based cells, was low with only 11% capacity loss within 3 days (see Figure S51, Supporting Information). This is comparable to or even better than published values for organic cathode materials.^[18,49] Extending the potential range to 4.1 V versus Li/Li^+ in the upper region allowed accessing a higher capacity for **P1a** (see Figure S54a, Supporting Information). However, a lower cycling stability resulted.

The conjugated polymer backbone in **P1a** and **P2** allowed for an ultra-high rate capability, as can be seen in the C-rate test in Figure 3e. Even at 100C, corresponding to a current density of 3.6 A g^{-1} (1.5 mA cm^{-2}), a specific capacity of 32.7 and 30.9 mAh g^{-1} was accessible for **P1a** and **P2**, corresponding to 90% and 85% of the theoretical value, respectively. In **P3**, on the other hand, where conjugation is interrupted, rates higher than 10C provided no capacity of the active material, and even at 10C rate, the capacity significantly declined within six cycles. Long-term cycling at 10C rate (for charge and discharge) showed that bithiophene copolymer **P1a** was superior to fluorene-based copolymer **P2** and non-conjugated polymer **P3** (Figure 3f). Over 2200 cycles, the capacity remained constant at a value of

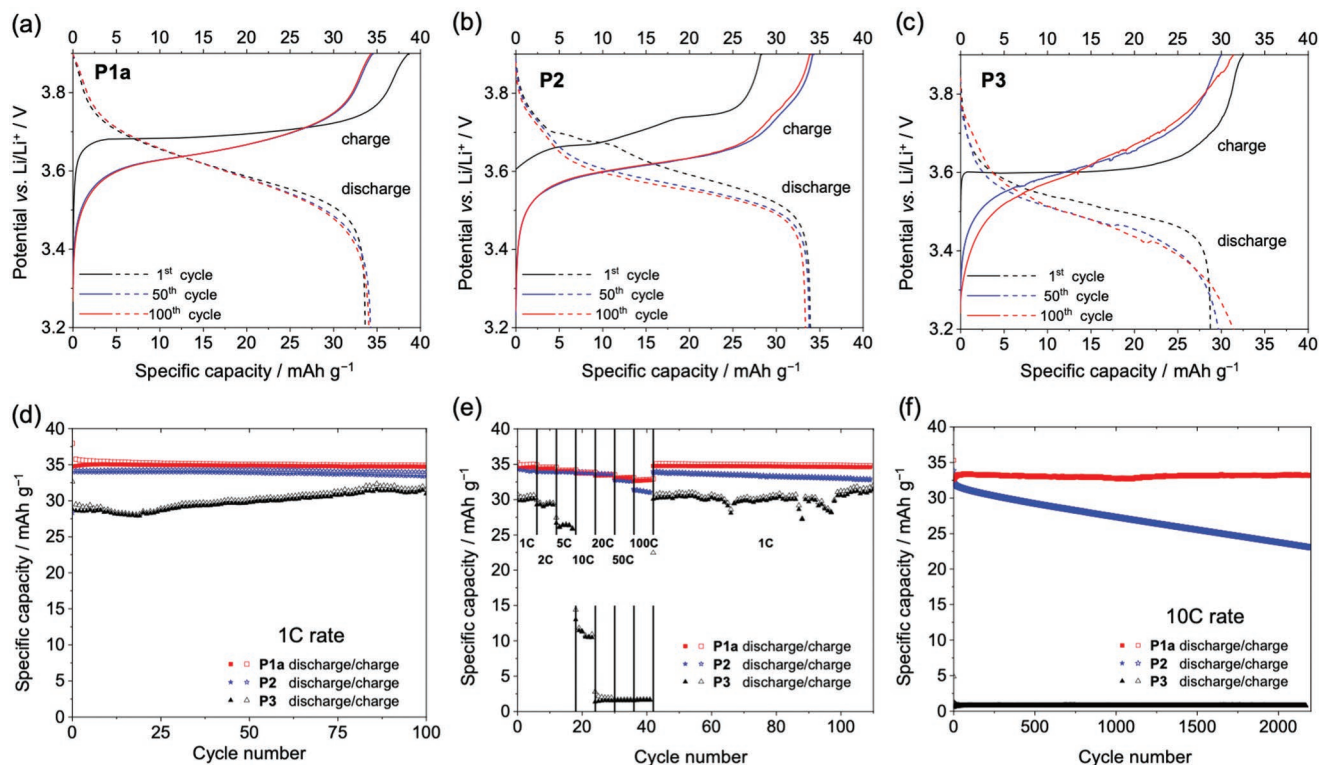


Figure 3. Cycling performance of **P1a**-, **P2**-, and **P3**-based composite electrodes: a–c) Selected charge/discharge curves of constant current cycling measurements at 1C rate; d) cycling stability at 1C rate; e) C-rate test; f) constant current cycling measurements at 10C.

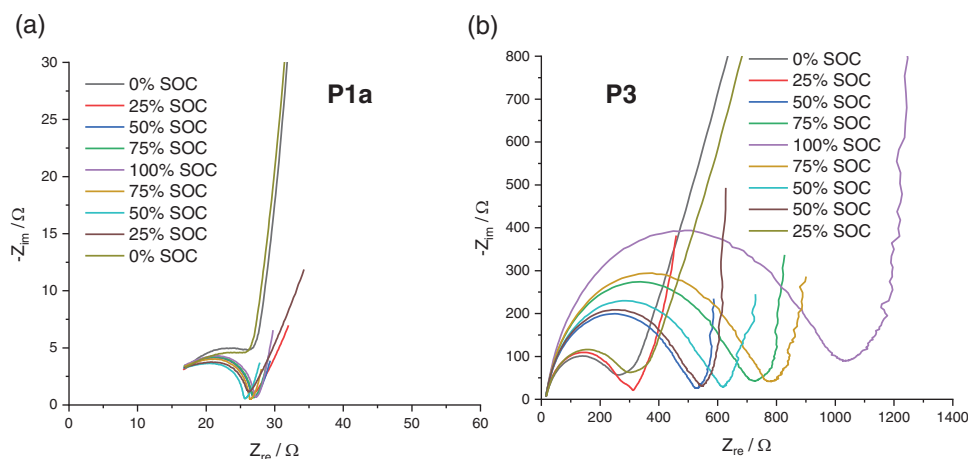


Figure 4. Nyquist plots from electrochemical impedance spectroscopy measurements of composite electrodes of polymers **P1a** (a) and **P3** (b) measured in different states of charge (SOC).

33.1 mAh g⁻¹. For **P2**, the capacity dropped to 72% of the initial value after 2200 cycles (23.0 mAh g⁻¹), while **P3** did not show any capacity of the active material at 10C rate. The same result was obtained from measurements of different cells. The higher cycling stability of bithiophene copolymer **P1a** compared to fluorene copolymer **P2** at 10C rate was likely due to the electron-donating and stabilizing effect of the bithiophene units on the oxidized phenothiazine groups in **P1a** compared to the fluorene units in **P2**.

As visible from electrochemical impedance spectroscopy (Figure 4 and Figure S55, Supporting Information), **P3**-based composite electrodes showed a significantly higher charge-transport resistance in the discharged state (0% SOC) of 259 Ω compared to **P1a** (24 Ω). With increasing state-of-charge, this resistance further increased in **P3** as did the double-layer capacitance due to the poor hole conduction of the material (965 Ω at 100% charge). In **P1a**-based composite electrodes, on the other hand, the charge-transport resistance decreased with increasing state-of-charge (14 Ω at 100% charge), demonstrating good hole conduction of the material.

Encouraged by these results, a long-term cyclization at the ultra-fast rate of 100C was performed with **P1a**-based composite electrodes. An excellent cycling stability was observed (Figure 5 and Figure S52, Supporting Information, for an average of three different cells). A maximum capacity of 30.1 mAh g⁻¹ (83% of the theoretical value) was reached after 15 000 cycles, which only dropped by 2.5% up to cycle 30 000. The charge/discharge curves showed that even at this high rate, plateau potentials were obtained with a value of 3.6 V versus Li/Li⁺ for the discharge (Figure 5b). The differential capacity plots (see Figure S49, Supporting Information) showed well-defined peaks for charge and discharge. The specific energy of the final discharge cycle 30 000 amounted to 108.4 Wh kg⁻¹, corresponding to a specific power of 10 836 W kg⁻¹ of the active material. This is remarkable in comparison to established inorganic cathodes for lithium batteries^[50] with specific energies of 80–250 Wh kg⁻¹ and specific power values of 200–4500 W kg⁻¹, which often times have a cycle life of only up to 2000 full charge/discharge cycles.^[50,51] To the best of our knowledge, such a fast and long-term cycling stability at a potential of 3.6 V versus Li/Li⁺

is unprecedented for organic cathode materials. A literature survey (see Supporting Information for details) showed that organic electrodes with the highest reported rate capabilities employing at least 25 wt% active material and with discharge potentials ≥3.4 V were based on TEMPO (2,2,6,6-tetramethylpiperidinyl-N-oxyl),^[52,53] phenothiazine^[28,29] or triaryl amines^[54–56] as redox-active groups. However, a long-term cyclization at 100C has been reported only once with 5000 cycles and a material loading of 40 wt%.^[54] We ascribe these results to the conjugated copolymer structure, where defined redox processes take place, but at the same time hole conduction along the polymer backbone is possible. As we will show later through substituent modification, the aryl ether group on the phenothiazine and the alkyl groups on the bithiophene units provided an ideal compromise between well-defined phenothiazine redox centers and a sufficient degree of conjugation along the polymer backbone.

2.1.4. Mechanistic Investigation of Charge/Discharge Processes in **P1a** and **P2**

We next investigated whether the observed redox processes in **P1a**- and **P2**-based cells were faradaic or capacitive in nature because their ultra-high rate capability was reminiscent of capacitors. The CVs, featuring distinct oxidative and reductive peaks (Figure 2), and the charge/discharge curves with well-defined plateaus (Figures 3 and 5) provided evidence for a battery-type behavior.^[57] The differential capacity plots (see Figure S49, Supporting Information) showed narrow and well-defined peaks for **P1a** and **P2**, even at the fast rate of 100C for **P1a**, which further underlines the faradaic nature of the redox processes. Furthermore, the change of the current i with the scan rate v at a fixed potential, as extracted from the CVs at different scan rates, was investigated. The relationship between the peak current i and v can be expressed as

$$i = kv^b \quad (1)$$

where k and b are adjustable parameters.^[58] It has been suggested that if b has a value of 0.5, the process can be considered

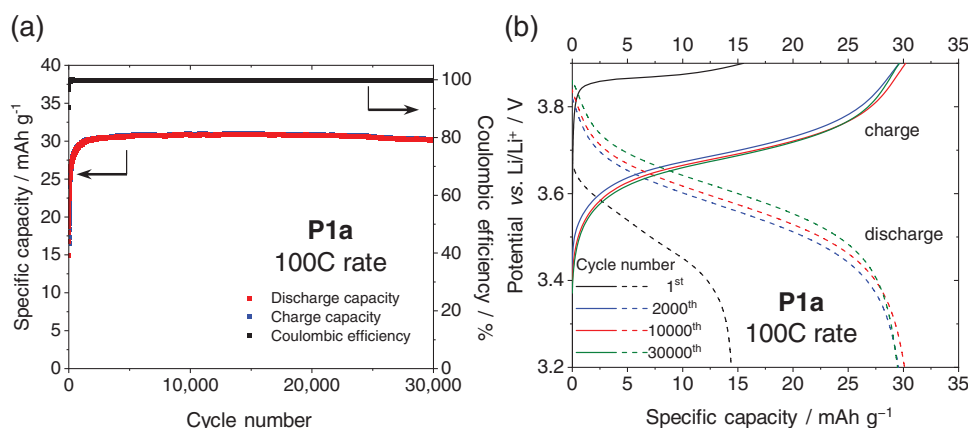


Figure 5. Constant current cycling measurement at 100C rate for **P1a** (a) with selected charge/discharge curves (b).

faradaic, while if b equals 1, the process is capacitive.^[58] Evaluating the peak current for oxidation and reduction (plotting $\log(i)$ vs $\log(v)$) resulted in b -values of 0.55 for **P1a** and 0.51 for **P2**, demonstrating the faradaic nature of the redox processes (Figure S48, Supporting Information).

With the calculated k -values in hand, the capacitive contribution to the total current at a fixed potential V was evaluated using the equation^[59]

$$i(V) = k_1 v + k_2 v^{0.5} \quad (2)$$

As can be seen in Figure 6, the capacitive contribution was very low for the redox process of both **P1a** and **P2**. In particular in **P1a**-based cells, 91% of the capacity stemmed from faradaic processes.

Calculations served to rationalize the different cycling behavior of polymers **P1a** and **P2**. In benchmark calculations, we chose oligomer model systems **O1a** and **O2** for polymers **P1a** and **P2**, respectively, containing two repeating units of the respective polymer with symmetric endings (see Figure 7 and Supporting Information for details). Calculations were performed at the wB97XD^[60]/6-31G(d)^[61,62] theory level for structure optimizations followed by single-point energy calculations at the wB97XD/6-311G(d,p)^[63–65] theory level for the density of

states (DOS, obtained using the AOMix package^[66,67]) and spin-density (for further detail see Supporting Information).

The DOS (Figure 7a) shows that for **O1a**, both bithiophene and phenothiazine moieties contributed to the HOMO composition (DOS between -6 and -8 eV). For **O2**, on the other hand, the major contribution stemmed from the phenothiazine units, while the fluorene moieties played a negligible role. This indicated a higher conjugation degree for **O1a** than for **O2**, which could explain the higher rate capability of **P1a** compared to **P2**. The spin densities obtained for the first oxidized state are shown in Figure 7b. Both are mostly localized on the phenothiazine units.

In all three oligomer model structures **O1a**, **O2**, and **O3**, the phenothiazine unit planarized upon oxidation from a “butterfly” angle of about 149° to close to 180° (see Supporting Information for details). In addition, in **O1a**, the torsional angle between the phenothiazine groups and the adjacent thiophenyl groups became smaller (54° to 35°). This is in line with the enhanced conjugation in polymer **P1a**.

2.2. Influence of Side Chains on the Cell Performance of P1

Based on the excellent rate performance and cycling stability of bithiophene-based polymer **P1a**, we next aimed to increase its

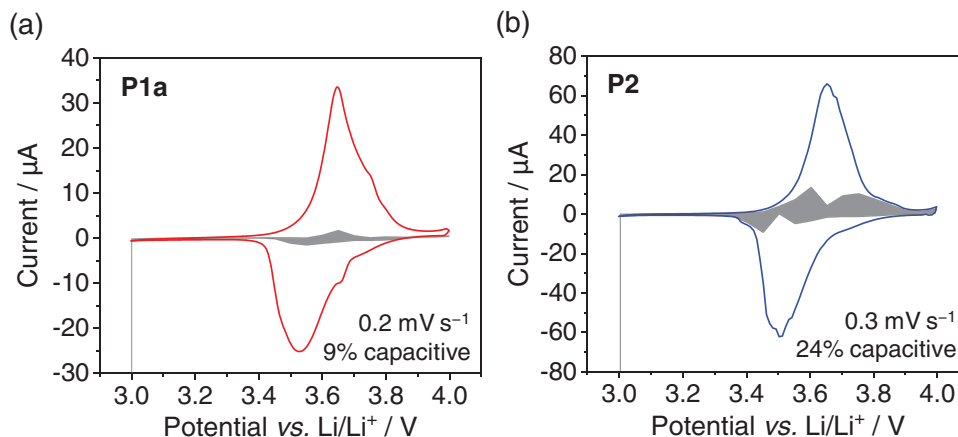


Figure 6. Cyclic voltammograms of **P1a**- and **P2**-based composite electrodes with the capacitive contribution highlighted in grey.

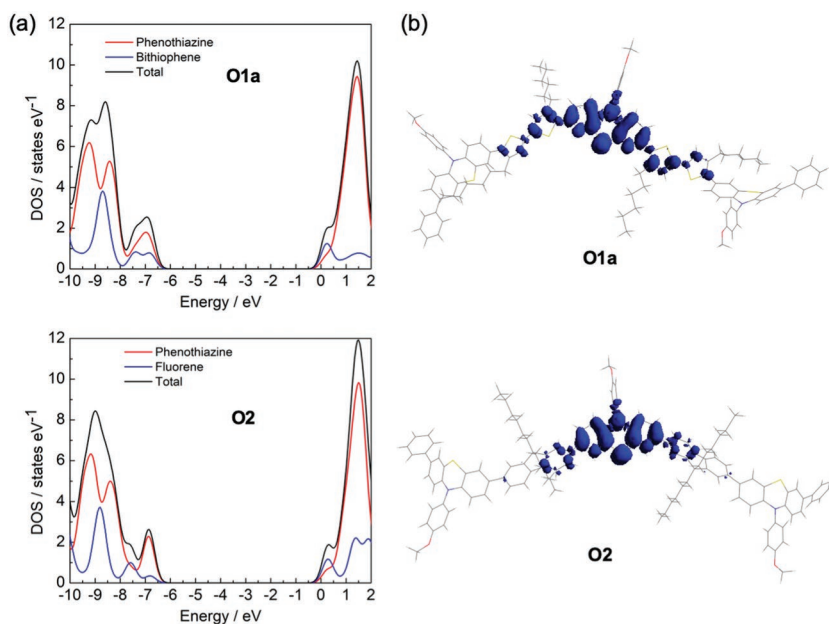


Figure 7. Computational results for oligomer model systems **O1a** and **O2** (wB97XD/6-311G(d,p)): a) total and partial densities of states (DOS) and b) spin densities for the first oxidized state (isovalue = 0.001).

specific capacity by decreasing the lengths or amount of alkyl side chains and synthesized polymers **P1b–d** (Scheme 2). In polymer **P1b**, all alkyl chains were removed apart from a methyl group at the nitrogen atom. In **P1c** and **P1d**, the aryl ether unit on the nitrogen was maintained, but the branched alkyl chain was replaced with a methyl group. In **P1c**, the bithiophene groups remained unsubstituted, while in **P1d**, methyl substituents were

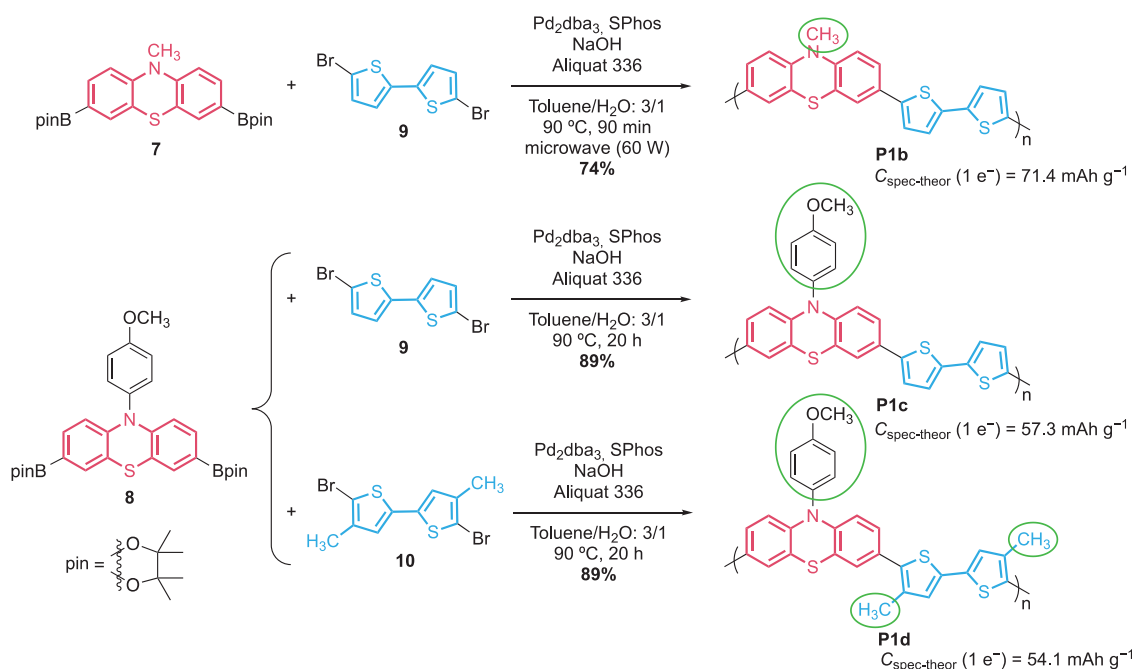
attached. This furthermore allowed us to assess the influence of substituents on the cycling behavior of the polymers, resulting from electronic and conformational differences.

2.2.1. Synthesis of Polymers **P1b–d**

The syntheses of **P1b–d** employed phenothiazine monomers **7** and **8** together with bithiophene monomers **9** and **10**, as shown in Scheme 2. Polycondensations were performed using the optimized Suzuki–Miyaura conditions, as discussed above for **P1a**, **P2**, and **P3**. The resulting polymers **P1b–d** were insoluble in common organic solvents due to the lack of alkyl side chains and precipitated from the reaction mixture. Hence, molecular weights could not be determined. Consecutive Soxhlet extraction with methanol, acetone, ethyl acetate, and dichloromethane allowed obtaining the polymers in sufficient purity for battery cell measurements.

2.2.2. Investigation of Polymers **P1b–d** as Cathode-Active Battery Materials

To investigate **P1b–d** as cathode-active materials in batteries, we fabricated composite electrodes as described for **P1a**, **P2**, and **P3** above in the ratio of 60 wt% polymer, 35 wt% Super C65 as conductive additive, and 5 wt% PVdF binder. With values of



Scheme 2. Synthesis of phenothiazine-bithiophene copolymers **P1b–d** with theoretical specific capacities.

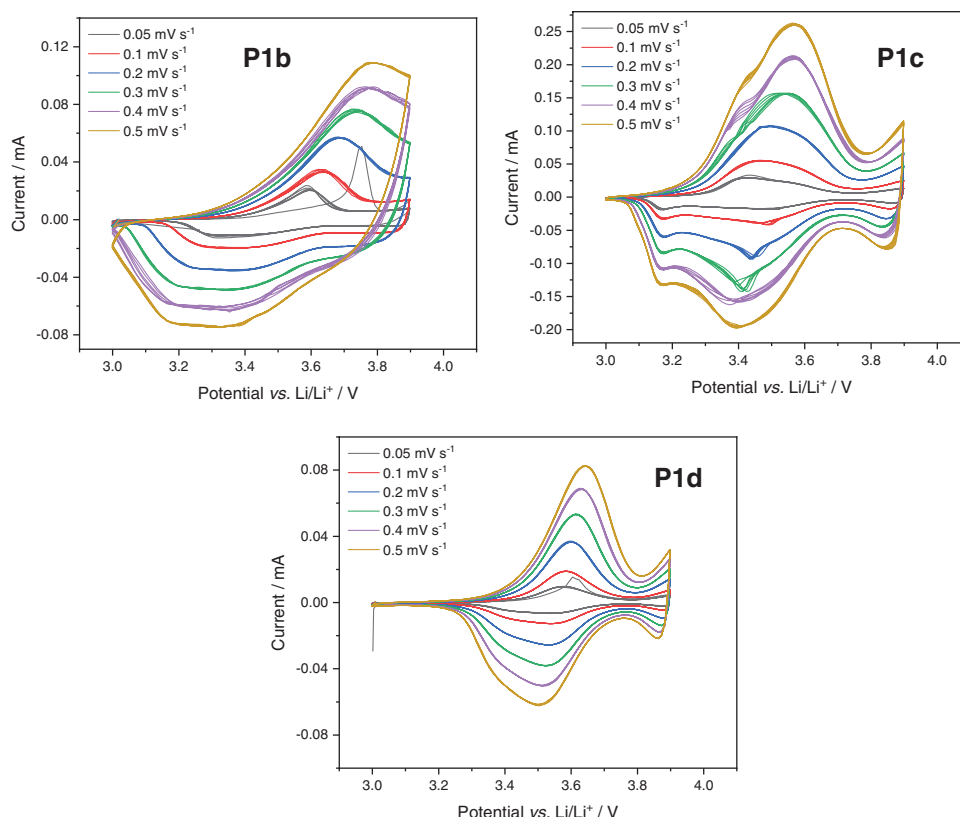


Figure 8. Cyclic voltammograms of **P1b–d** in composite electrodes at different scan rates (polymer/carbon black/PVdF (60:35:5 wt%), 1 M LiPF₆ in EC/DMC (1:1), counter/reference electrode: Li foil).

71.4 mAh g⁻¹ for **P1b**, 57.3 mAh g⁻¹ for **P1c**, and 54.1 mAh g⁻¹ for **P1d**, the theoretical specific capacities are significantly higher than for **P1a**.

In cyclic voltammograms in composite electrodes, **P1b** showed a somewhat narrow oxidation peak but a broad re-reduction peak on the cathodic scan and a large peak separation (Figure 8). This likely resulted from the stronger conjugation between the phenothiazine and bithiophene units due to the absence of alkyl chains. Similar electrochemical behavior has been observed in phenothiazine homopolymers.^[31] A calculation on the radical cation of the corresponding model compound **O1b** revealed that the spin density was mostly localized on a bithiophene unit and only half of the adjacent phenothiazine groups (Figure 9b). As a result, the phenothiazine units did not planarize upon oxidation (Figure 9a). This stands in contrast to aryl ether-substituted **O1a**, **O1c**, and **O1d**, where the radical cation was centrally localized on the phenothiazine units, which, as a consequence, planarized upon oxidation (see Figure 9 and Figure S80, Supporting Information). Hence, in polymer **P1b**, the bithiophene groups significantly partook in the oxidation reaction.^[68]

In **P1c** and **P1d**, containing an aryl ether substituent on the phenothiazine group, the oxidations were more defined (Figure 8). This had also been the case for **P1a** (see Figure 2) and is in line with the calculated planarization of the phenothiazine units upon oxidation in all three model compounds **O1a**, **O1c**, and **O1d** (see Figure 9). Introducing alkyl substituents

on the bithiophene units led to a further narrowing of the redox peaks in **P1d** (see also **P1a** in Figure 2). This localization of charges due to the presence of alkyl substituents in thiophene copolymers has been demonstrated in other contexts before.^[69,70]

In constant current cycling measurements, **P1b**, featuring the highest theoretical capacity, provided the highest specific capacity at 1C rate, while **P1d** showed the best rate capability (Figure 10). At 1C rate, all three polymers demonstrated stable cycling behavior. For **P1b**, a reversible capacity of 56.9 mAh g⁻¹ was accessible, which amounted to 80% of the theoretical value for a one-electron oxidation (the theoretical capacities can be found in Scheme 2). For **P1c**, 41.0 mAh g⁻¹ were accessible (72% of the theoretical value), and for **P1d**, 38.9 mAh g⁻¹ (72% of the theoretical value). The incomplete capacity use in these polymers was likely either due to the presence of polymer agglomerates in the composite electrode caused by their insolubility during processing (for SEM images, see Figures S71–S76, Supporting Information) or to the fact that the polymer chains were short and electrochemically inactive end groups reduced the specific capacities. Extending the potential range to 4.1 V versus Li/Li⁺ in the upper region allowed accessing higher capacities for all three polymers **P1b–d** with stable cycling at 1C rate for **P1b** and **P1c** (see Figure S54b–d, Supporting Information).

The charge/discharge curves (Figure 10d–f) demonstrated a behavior similar to the CVs shown in Figure 8; for **P1b** and **P1c**,

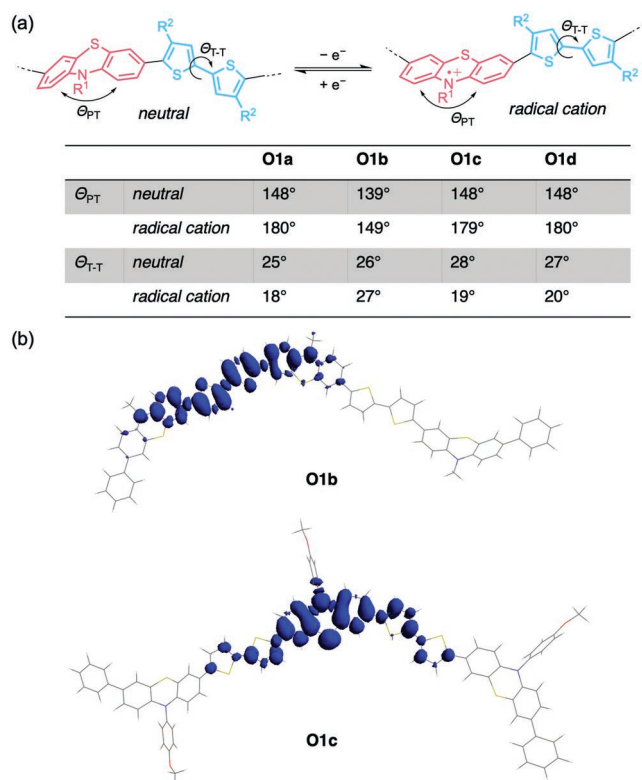


Figure 9. a) Selected calculated torsional angles (wB97XD/6-31G(d)) for oligomer model systems **O1a–d** in the neutral and radical cation state. b) Calculated spin densities (wB97XD/6-311G(d,p)) for the first oxidized state of **O1b** and **O1c** (isovalue = 0.001).

sloping potential curves were obtained, while **P1d** showed more defined plateaus. This again can be explained by the presence of the methyl groups on the bithiophene units in **P1d**, which had a pronounced influence on the localization of charges on the phenothiazine units.

P1d featured the best rate performance followed by **P1c** and **P1b** (Figure 10). For **P1d**, a capacity of 31.5 mAh g⁻¹ was accessible at 100C rate (Figure 10c). The rate capability of **P1c** was also good, which again can be traced back to the presence of the aryl ether groups on the phenothiazine units. The poorer rate performance of **P1b**, on the other hand, might be due to 1) the missing planarization of the phenothiazine groups upon oxidation and 2) the larger torsional angle between the thiophene units in the oxidized form compared to **P1c** and **P1d** (see Figure 9).

In summary, in spite of the larger amount of inactive mass in **P1a** compared to **P1b–d**, this polymer showed the best performance regarding accessible capacity, rate capability, and cycling stability. This was due to the electronic effects of the aryl ether group, the steric influence of the bithiophene alkyl groups on the polymer conformation, as well as its high solubility, which allowed for good processing of the composite electrodes. The long alkyl groups in **P1a** likely favor formation of an amorphous phase in the composite electrode, which accelerates counter ion diffusion, a phenomenon, which has been observed in other redox-active polymers before.^[71]

3. Conclusions

In conclusion, we have shown that using a π -conjugated copolymer structure enabled ultra-high rate capability and cycling stability at 100C rate in phenothiazine-based polymers as cathode-active battery materials. Best results were achieved with **P1a**, possessing alternating phenothiazine and bithiophene units. We ascribe this to the semiconducting nature of **P1a**, which allowed for fast charge transport in the composite electrode. Yet, due to the copolymer structure, localized phenothiazine redox centers were maintained along the polymer chain, which resulted in well-defined plateau potentials on charge and discharge at 3.6 V versus Li/Li⁺, close to the operating potential of commercial Li-ion battery cathodes. The redox processes were mostly faradaic in nature (>90%). Calculations showed that a slightly higher degree of conjugation in **P1a** compared to fluorene-based copolymer **P2** was likely responsible for its superior rate performance. A comparison with polymers **P1c–d** carrying fewer and smaller substituents demonstrated that both the aryl ether as well as the alkyl substituents in **P1a** were necessary to obtain this outstanding behavior. We believe that this concept of using a π -conjugated copolymer structure is attractive for applications, where a high rate performance of the electrode is required.

4. Experimental Section

Synthetic Procedures: Further details on materials and methods as well as synthetic procedures for compounds **1–10** and computational details can be found in Supporting Information.

Microwave reactions were conducted in a *Discover S-class* microwave oven from CEM. NMR spectra were recorded at room temperature on a Bruker Avance III HD 500, Bruker Avance Neo 400, Bruker Avance II 400, or Bruker Avance III HD 300 spectrometer. Chemical shifts were reported in parts per million (ppm, δ scale). The ¹H and ¹³C spectra were calibrated against the residual proton and natural abundance ¹³C resonances of CDCl₃ (¹H: 7.26 ppm, ¹³C: 77.16 ppm) or against TMS (¹H, ¹³C: 0 ppm). The following abbreviations were used: s = singlet, d = doublet, t = triplet, m = multiplet, and br = broad. The coupling constants (J) were indicated in Hertz (Hz). Analytical gel permeation chromatography was performed on a SECcurity GPC System from PSS Polymer Standard Service using components of the 1260 Infinity series from Agilent Technologies (IsoPump: G1310B, auto sampler: ALS G1329B, UV-detector: MWD VL G1365D, RI-detector: RID G1362A). Three columns were used (PSS SDV, 8 mm × 300 mm with a porosity of 10², 10³, and 10⁵ with integrated pre-column). As eluent, degassed THF was used with a flow rate of 1 mL min⁻¹. A polystyrene standard by PSS was used for calibration. For TGA, a STA 409 or a STA 449 F5 by Netzsch and for DSC a Netzsch DSC 204 F1 Phoenix were used. UV–vis absorption and emission spectra were recorded on a Tidas I or Tidas II diode array spectrometer from J&M Analytik AG, and on a Perkin Elmer LS55 in a 10 mm fused quartz cuvette. Cyclic voltammetry in solution was performed inside of a glovebox using a Metrohm Autolab PGSTAT 128N. As working electrode, a glassy carbon disc electrode (2 mm diameters) was used. A platinum rod served as counter electrode, and as reference electrode, a Ag/AgNO₃ electrode containing a silver wire immersed in an inner chamber filled with 0.1 M AgNO₃ containing 0.1 M *n*-Bu₄NPF₆ in the outer chamber was used. For the internal reference, the ferrocene/ferrocenium (Fc/Fc⁺) redox couple was used.

General Method for the Suzuki Polycondensation (Microwave Assisted): The following optimized method was used for polymers **P1a**, **P2**, **P3**, and **P1b** (the amounts of reagents and solvents are detailed for each polymer below). Phenothiazine diboronic ester **1** or **7**, the respective

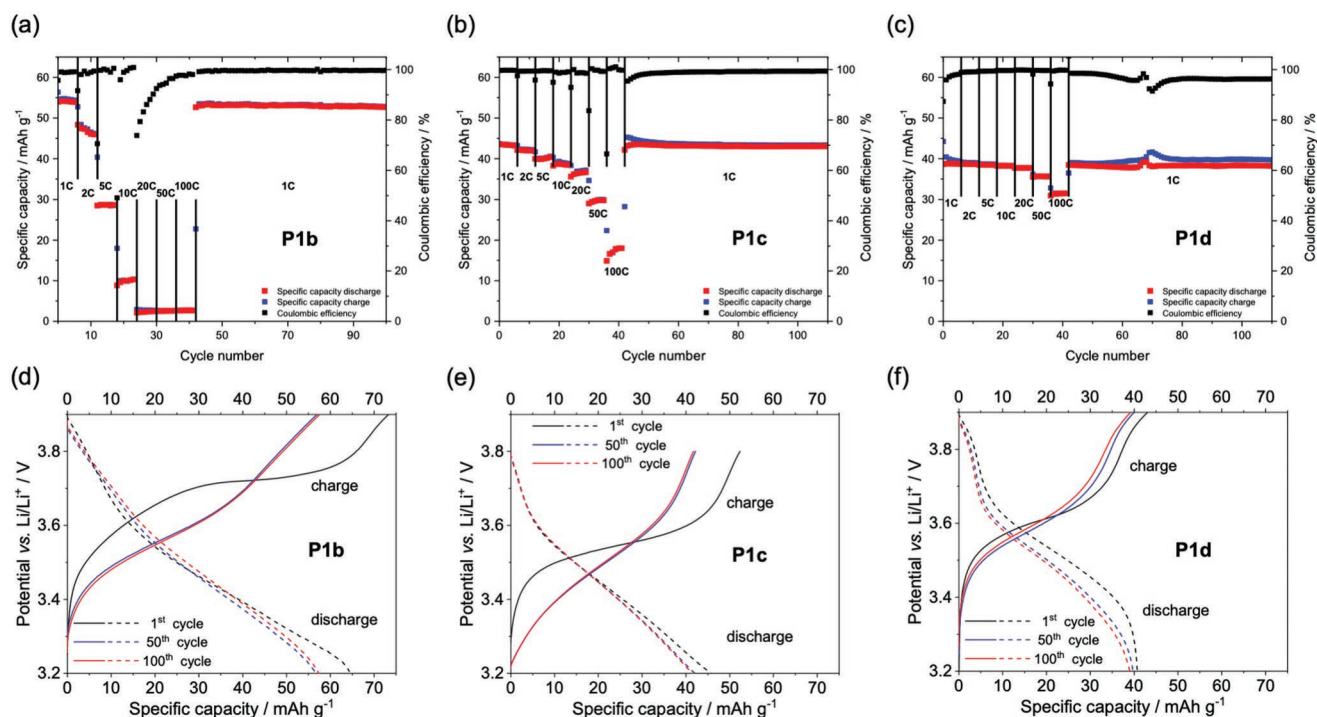


Figure 10. Cycling performance of **P1b–d**-based composite electrodes: a–c) C-rate tests; d–f) selected charge/discharge curves of constant current cycling measurements at 1C rate (polymer/carbon black/PVDF (60:35:5 wt%), 1 M LiPF₆ in EC/DMC (1:1), counter/reference electrode: Li foil).

dibromo-compound **4**, **5**, **6**, or **9**, Aliquat 336, NaOH, Pd₂dba₃, and SPhos were dissolved in degassed toluene. Argon-saturated H₂O was added. The vessel was placed in the microwave reactor with the following settings: SPS-mode, 60 W, 90 °C, 30–90 min (depending on solvent volume) with air cooling on. After completion of the reaction time, 4,4,5,5-tetramethyl-2-phenyl-1,3,2-dioxaborolane was added and left to react for 4 min and bromobenzene was added, and the reaction was stirred for another 4 min (same microwave conditions as before). Then the mixture was precipitated from cold acetone. The filtered polymer was redissolved and precipitated from methanol and dried in vacuum.

Synthesis of P1a: The general procedure for the Suzuki polycondensation (microwave assisted) was followed using phenothiazine monomer **1** (0.53 g, 0.81 mmol), bithiophene monomer **4** (0.40 g, 0.81 mmol), Pd₂dba₃ (29.2 mg, 32.0 μmol, 4 mol%), SPhos (25.3 mg, 62.0 μmol, 7.7 mol%), NaOH (0.35 g, 8.80 mmol, 11.0 eq.), toluene (6 mL), H₂O (2 mL), and Aliquat 336 (2–3 drops). Polymer **P1a** (0.59 g, 99%) was obtained as a yellow solid. ¹H NMR (400 MHz, CDCl₃): δ 7.34–7.31 (m, 2H), 7.15–7.13 (m, 2H), 7.07 (d, *J* = 2.1 Hz, 2H), 6.96 (s, 2H), 6.89 (dd, *J* = 8.8, 2.0 Hz, 2H), 6.21 (d, *J* = 8.6 Hz, 2H), 3.94–3.93 (m, 2H), 2.58–2.54 (m, 4H), 1.84–1.74 (m, 1H), 1.60–1.43 (m, 8H), 1.39–1.35 (m, 4H), 1.33–1.22 (m, 12H), 1.00–0.96 (m, 3H), 0.95–0.92 (m, 3H), 0.89–0.86 (m, 6H); ¹³C NMR (101 MHz, CDCl₃): δ 159.4, 143.6, 139.3, 135.6, 135.1, 132.7, 132.1, 128.8, 127.8, 127.1, 125.9, 119.5, 116.7, 115.7, 71.0, 39.6, 31.8, 31.0, 30.7, 29.3, 29.3, 29.0, 24.1, 23.2, 22.8, 14.3 (2C), 11.3; anal. GPC (eluent THF, polystyrene standard): *M*_n = 3.29 · 10⁴ g mol^{−1}, PDI 2.65; TGA_{onset} (10 °C min^{−1}, O₂): 405 °C.

Synthesis of P2: The general procedure for the Suzuki polycondensation (microwave-assisted) was followed using phenothiazine monomer **1** (68.6 mg, 0.11 mmol), fluorene monomer **5** (51.5 mg, 0.11 mmol), Pd₂dba₃ (3.80 mg, 4.2 μmol, 4 mol%), SPhos (3.40 mg, 8.40 μmol, 8 mol%), NaOH (46.0 mg, 1.15 mmol, 11.0 eq.), toluene (3 mL), H₂O (1 mL), and Aliquat 336 (2–3 drops). Polymer **P2** (49.8 mg, 65%) was obtained as a green solid. ¹H NMR (400 MHz, CDCl₃): δ 7.70–7.68 (m, 2H), 7.47–7.44 (m, 4H), 7.37–7.32 (m, 4H), 7.17–7.14 (m, 4H), 6.31–6.29 (m, 2H), 3.97–3.92 (m, 2H), 2.04–1.97 (m, 4H), 1.85–1.77 (m, 1H),

1.64–1.45 (m, 4H), 1.43–1.37 (m, 4H), 1.16–0.94 (m, 18H), 0.78–0.75 (m, 6H), 0.71–0.62 (m, 4H); ¹³C NMR (101 MHz, CDCl₃): δ 159.4, 151.8, 143.7, 140.0, 138.8, 136.0, 133.2, 132.2, 125.7, 125.3, 125.1, 120.8, 120.0, 119.8, 116.8, 116.1, 71.1, 55.4, 40.6, 39.7, 31.6, 30.8, 29.9, 29.3, 24.1, 24.0, 23.2, 22.7, 14.3, 14.1, 11.4; anal. GPC (eluent THF, polystyrene standard): *M*_n = 9.40 · 10⁴ g mol^{−1}, PDI 2.00; TGA_{onset} (10 °C min^{−1}, O₂): 402 °C.

Synthesis of P3: The general procedure for the Suzuki polycondensation (microwave-assisted) was followed using phenothiazine monomer **1** (70.6 mg, 0.11 mmol), thiophene monomer **6** (56.0 mg, 0.11 mmol), Pd₂dba₃ (3.90 mg, 4.26 μmol, 3.9 mol%), SPhos (3.60 mg, 8.77 μmol, 8 mol%), NaOH (42.0 mg, 1.05 mmol, 13.6 eq.), toluene (1.5 mL), H₂O (0.5 mL), and Aliquat 336 (2–3 drops). Polymer **P3** (53.8 mg, 99%) was obtained as a yellow solid. ¹H NMR (400 MHz, CDCl₃): δ 7.28–7.26 (m, 2H), 7.16 (d, *J* = 2.2 Hz, 2H), 7.12–7.10 (m, 2H), 6.97 (dd, *J* = 8.6, 2.2 Hz, 2H), 6.86 (s, 2H), 6.12 (d, *J* = 8.6 Hz, 2H), 3.93–3.92 (m, 2H), 3.00 (s, 4H), 2.44–2.41 (m, 4H), 1.83–1.74 (m, 1H), 1.62–1.42 (m, 8H), 1.40–1.34 (m, 4H), 1.32–1.21 (m, 12H), 0.99–0.96 (m, 3H), 0.95–0.92 (m, 3H), 0.88–0.85 (m, 6H); ¹³C NMR (101 MHz, CDCl₃): δ 159.3, 143.2, 139.8, 139.2, 136.0, 132.9, 132.1, 129.2, 124.1, 123.9, 123.4, 119.6, 116.6, 115.8, 71.0, 39.6, 31.9, 31.0, 30.7, 30.6, 29.5, 29.3, 28.6, 24.1, 23.2, 22.8, 14.3 (2C), 11.3; anal. GPC (eluent THF, polystyrene standard): *M*_n = 1.89 · 10⁴ g mol^{−1}, PDI 2.47; TGA_{onset} (10 °C min^{−1}, O₂): 402 °C.

Synthesis of P1b: The general procedure for the Suzuki polycondensation (microwave-assisted) was followed using phenothiazine monomer **7** (0.20 g, 0.43 mmol), thiophene monomer **9** (0.14 g, 0.43 mmol), Pd₂dba₃ (0.02 g, 0.02 mmol, 4 mol%), SPhos (0.01 g, 0.03 mmol, 8 mol%), NaOH (0.19 g, 4.73 mmol, 11.0 eq.), toluene (4 mL), H₂O (1 mL), and Aliquat 336 (2–3 drops). For further purification the polymer was Soxhlet-extracted with MeOH, acetone, EtOAc, and CH₂Cl₂. Polymer **P1b** (0.12 g, 74%) was obtained as a red solid. TGA_{onset} (10 °C min^{−1}, O₂): 410 °C.

Synthesis of P1c: The general procedure for the Suzuki polycondensation (instead of microwave heating an oil bath was used (20 h, 90 °C)) was followed using phenothiazine monomer **8** (1.00 g, 1.79 mmol), thiophene monomer **9** (0.58 g, 1.79 mmol), Pd₂dba₃ (0.07 g, 0.07 mmol, 4 mol%), SPhos (0.06 g, 0.14 mmol, 8 mol%),

NaOH (0.79 g, 19.7 mmol, 11 eq.), toluene (20 mL), H₂O (5 mL), and Aliquat 336 (5 drops). For further purification the polymer was Soxhlet-extracted with MeOH, acetone, EtOAc, and CH₂Cl₂. Polymer P1c (0.75 g, 89%) was obtained as a red solid. TGA_{onset} (10 °C min⁻¹, O₂): 337 °C.

Synthesis of P1d: The general procedure for the Suzuki polycondensation (instead of microwave heating an oil bath was used (20 h, 90 °C)) was followed using phenothiazine monomer **8** (1.00 g, 1.79 mmol), thiophene monomer **10** (0.63 g, 1.79 mmol), Pd₂dba₃ (0.07 g, 0.07 mmol, 4 mol%), SPhos (0.06 g, 0.14 mmol, 8 mol%), NaOH (0.79 g, 19.7 mmol, 11 eq.), toluene (20 mL), H₂O (5 mL), and Aliquat 336 (5 drops). For further purification the polymer was Soxhlet-extracted with MeOH, acetone, EtOAc, and CH₂Cl₂. Polymer P1d (0.79 g, 89%) was obtained as a green solid. TGA_{onset} (10 °C min⁻¹, O₂): 378 °C.

Fabrication of Composite Electrodes: Composite electrodes were prepared using 60 wt% polymer, 35 wt% carbon black (Super C65, Timical), and 5 wt% binder (PVdF, Solef 5130) immersed in 1-methyl-2-pyrrolidone (NMP, 99.5%, ACROS Organics, stored over molecular sieves). The mixtures were stirred for 12 h at room temperature. Because of inhomogeneous particle sizes, the mixture for **P1d** was additionally homogenized using a ball mill (Pulverisette 7 from Fritsch). The resulting paste was blade-coated onto KOH-etched aluminum foil (1235 aluminum foil, H18 hard state, 20 µm from Gelon LIB), resulting in a wet-film thickness of 100 µm. The coated aluminum foil was dried at 80 °C in a vacuum oven at 10⁻² mbar, and electrodes with a diameter of 12 mm were punched out with an electrode-punching device (coin cell punching machine GN-T06 from Gelon LIB). The dried electrodes showed film thicknesses for **P1a** of 10–18 µm, for **P2** of 16–26 µm, for **P3** of 23–26 µm, for **P1b** of 10–20 µm, for **P1c** of 26–35 µm, and for **P1d** of 20–30 µm (measured with a Mitutoyo MT547-400S thickness gage), and the mass loadings lay between 0.10 mg and 1.10 mg per electrode (1.13 cm²).

Electrochemical Characterization and Analysis: Three-electrode Swagelok T-cells were assembled in an Ar-filled glovebox (UNILAB 230V from MBraun) containing less than 0.1 ppm of water and oxygen. Lithium (Alfa Aesar, 99.9%) foil was used as counter (Ø = 12 mm) and reference electrode (Ø = 5 mm). Six layers of Freudenberg 2190 nonwoven PP separators were placed between the electrodes (1 M LiPF₆ in EC/DMC: 1/1, BASF Selectilyte, 120 µL). Cyclic voltammetry and galvanostatic cycling measurements on these cells were conducted on a MPG-2 potentiostat from BioLogic Science Instruments.

Supporting Information

Supporting Information is available from the Wiley Online Library or from the author.

Acknowledgements

P.A. thanks J. Haxhija and F. Hilfinger for preparative assistance, S. Küspert and A. Becherer for SEM measurements, and Prof. B. Breit for use of the microwave synthesizer. Financial support through the German Federal Environmental Foundation (DBU, graduate fellowship for P.A.), the German Research Foundation (DFG, Emmy Noether grant ES 361/2-1 for B.E.), the Swedish Energy Agency (C.M.A. and C.F.N.M., grant number 45420-1), STandUP for Energy, and Carl Tryggers Stiftelse is gratefully acknowledged. The theoretical calculations were done using the infrastructure provided by the Swedish National Infrastructure for Computing (SNIC) at the National Supercomputer Centre at Linköping University (NSC).

Conflict of Interest

The authors declare no conflict of interest.

Keywords

conjugated polymers, microwave chemistry, organic batteries, phenothiazine, redox chemistry

Received: August 6, 2019
Published online: September 1, 2019

- [1] H. Nishide, K. Oyaizu, *Science* **2008**, 319, 737.
- [2] H. Nishide, K. Koshika, K. Oyaizu, *Pure Appl. Chem.* **2009**, 81, 1961.
- [3] Y. Liang, Z. Tao, J. Chen, *Adv. Energy Mater.* **2012**, 2, 742.
- [4] T. Janoschka, M. D. Hager, U. S. Schubert, *Adv. Mater.* **2012**, 24, 6397.
- [5] Z. Song, H. Zhou, *Energy Environ. Sci.* **2013**, 6, 2280.
- [6] Z. Zhu, J. Chen, *J. Electrochem. Soc.* **2015**, 162, A2393.
- [7] Y. Zhang, J. Wang, S. N. Riduan, *J. Mater. Chem. A* **2016**, 4, 14902.
- [8] J. Xie, Q. Zhang, *J. Mater. Chem. A* **2016**, 4, 7091.
- [9] T. B. Schon, B. T. McAllister, P.-F. Li, D. S. Seferos, *Chem. Soc. Rev.* **2016**, 45, 6345.
- [10] Q. Zhao, Y. Lu, J. Chen, *Adv. Energy Mater.* **2017**, 7, 1601792.
- [11] S. Lee, G. Kwon, K. Ku, K. Yoon, S.-K. Jung, H.-D. Lim, K. Kang, *Adv. Mater.* **2018**, 1704682.
- [12] Y. Liang, Y. Yao, *Joule* **2018**, 2, 1690.
- [13] M. Armand, J.-M. Tarascon, *Nature* **2008**, 451, 652.
- [14] P. Poizat, F. Dolhem, *Energy Environ. Sci.* **2011**, 4, 2003.
- [15] P. Novák, K. Müller, K. S. V. Santhanam, O. Haas, *Chem. Rev.* **1997**, 97, 207.
- [16] J. F. Mike, J. L. Lutkenhaus, *ACS Macro Lett.* **2013**, 2, 839.
- [17] R. Gracia, D. Mecerreyes, *Polym. Chem.* **2013**, 4, 2206.
- [18] S. Muench, A. Wild, C. Friebe, B. Häupler, T. Janoschka, U. S. Schubert, *Chem. Rev.* **2016**, 116, 9438.
- [19] M. E. Speer, M. Kolek, J. J. Jassoy, J. Heine, M. Winter, P. M. Bieker, B. Esser, *Chem. Commun.* **2015**, 51, 15261.
- [20] E. P. Tomlinson, M. E. Hay, B. W. Boudouris, *Macromolecules* **2014**, 47, 6145.
- [21] K. Oyaizu, H. Nishide, *Adv. Mater.* **2009**, 21, 2339.
- [22] K. Nakahara, K. Oyaizu, H. Nishide, *Chem. Lett.* **2011**, 40, 222.
- [23] H. E. Katz, P. C. Searson, T. O. Poehler, *J. Mater. Res.* **2010**, 25, 1561.
- [24] J. Xie, P. Gu, Q. Zhang, *ACS Energy Lett.* **2017**, 2, 1985.
- [25] V. Etacheri, R. Marom, R. Elazari, G. Salitra, D. Aurbach, *Energy Environ. Sci.* **2011**, 4, 3243.
- [26] Y. Liang, Z. Chen, Y. Jing, Y. Rong, A. Facchetti, Y. Yao, *J. Am. Chem. Soc.* **2015**, 137, 4956.
- [27] K. T. Sarang, A. Miranda, H. An, E.-S. Oh, R. Verduzco, J. L. Lutkenhaus, *ACS Appl. Polym. Mater.* **2019**, 1, 1155.
- [28] M. Kolek, F. Otteny, P. Schmidt, C. Mück-Lichtenfeld, C. Einholz, J. Becking, E. Schleicher, M. Winter, P. Bieker, B. Esser, *Energy Environ. Sci.* **2017**, 10, 2334.
- [29] F. Otteny, M. Kolek, J. Becking, M. Winter, P. Bieker, B. Esser, *Adv. Energy Mater.* **2018**, 1802151.
- [30] A. A. Golriz, T. Suga, H. Nishide, R. Berger, J. S. Gutmann, *RSC Adv.* **2015**, 5, 22947.
- [31] T. Godet-Bar, J.-C. Leprêtre, O. Le Bacq, J.-Y. Sanchez, A. Deronzier, A. Pasturel, *Phys. Chem. Chem. Phys.* **2015**, 17, 25283.
- [32] B. M. Peterson, D. Ren, L. Shen, Y.-C. M. Wu, B. Ulgut, G. W. Coates, H. D. Abruña, B. P. Fors, *ACS Appl. Energy Mater.* **2018**, 1, 3560.
- [33] T. Shimizu, K. Yamamoto, P. Pandit, H. Yoshikawa, S. Higashibayashi, *Sci. Rep.* **2018**, 8, 579.
- [34] M. Kolek, F. Otteny, J. Becking, M. Winter, B. Esser, P. Bieker, *Chem. Mater.* **2018**, 30, 6307.
- [35] K. A. Narayana, M. D. Casselman, C. F. Elliott, S. Ergun, S. R. Parkin, C. Risko, S. A. Odom, *ChemPhysChem* **2015**, 16, 1179.

- [36] D.-H. Hwang, S.-K. Kim, M.-J. Park, J.-H. Lee, B.-W. Koo, I.-N. Kang, S.-H. Kim, T. Zyung, *Chem. Mater.* **2004**, 16, 1298.
- [37] X. Kong, A. P. Kulkarni, S. A. Jenekhe, *Macromolecules* **2003**, 36, 8992.
- [38] M. Łapkowski, S. Plewa, A. Stolarczyk, J. Dąbrowski, J. Sołoducho, J. Cabaj, M. Bartoszek, W. W. Sułkowski, *Electrochim. Acta* **2008**, 53, 2545.
- [39] S. Yamada, S. Park, S. Song, M. Heo, J. Y. Shim, Y. Jin, I. Kim, H. Lee, K. Lee, K. Yoshinaga, Y. Y. Kim, H. Suh, *Polymer* **2010**, 51, 6174.
- [40] W. Tang, T. Kietzke, P. Vernumamada, Z.-K. Chen, *J. Polym. Sci. Part A Polym. Chem.* **2007**, 45, 5266.
- [41] H. S. Yoo, D. H. Yun, T. W. Ko, Y. S. Park, J. W. Woo, *Adv. Mater. Res.* **2013**, 634–638, 2621.
- [42] M. Takahashi, K. Masui, H. Sekiguchi, N. Kobayashi, A. Mori, M. Funahashi, N. Tamaoki, *J. Am. Chem. Soc.* **2006**, 128, 10930.
- [43] R. Bernard, C. Barsu, P. L. Baldeck, C. Andraud, D. Cornu, J.-P. Scharff, P. Miele, *Chem. Commun.* **2008**, 3765.
- [44] B. W. D'Andrade, S. Datta, S. R. Forrest, P. Djurovich, E. Polikarpov, M. E. Thompson, *Org. Electron.* **2005**, 6, 11.
- [45] C. O. Laoire, E. Plichta, M. Hendrickson, S. Mukerjee, K. M. Abraham, *Electrochim. Acta* **2009**, 54, 6560.
- [46] T. J. J. Müller, A. W. Franz, C. S. Barkschat (née Krämer), M. Sailer, K. Meerholz, D. Müller, A. Colmann, U. Lemmer, *Macromol. Symp.* **2010**, 287, 1.
- [47] M. Sailer, A. W. Franz, T. J. J. Müller, *Chem. Eur. J.* **2008**, 14, 2602.
- [48] All Capacities Herein Are Reported per Mass of Active Material.
- [49] K. Nakahara, J. Iriyama, S. Iwasa, M. Suguro, M. Satoh, E. J. Cairns, *J. Power Sources* **2007**, 165, 398.
- [50] P. Meister, H. Jia, J. Li, R. Kloepsch, M. Winter, T. Placke, *Chem. Mater.* **2016**, 28, 7203.
- [51] S. F. Tie, C. W. Tan, *Renew. Sustain. Energy Rev.* **2013**, 20, 82.
- [52] S. Komaba, T. Tanaka, T. Ozeki, T. Taki, H. Watanabe, H. Tachikawa, *J. Power Sources* **2010**, 195, 6212.
- [53] J.-K. Kim, J.-H. Ahn, G. Cheruvally, G. S. Chauhan, J.-W. Choi, D.-S. Kim, H.-J. Ahn, S. H. Lee, C. E. Song, *Met. Mater. Int.* **2009**, 15, 77.
- [54] K. Yamamoto, D. Suemasa, K. Masuda, K. Aita, T. Endo, *ACS Appl. Mater. Interfaces* **2018**, 10, 6346.
- [55] C. Zhang, X. Yang, W. Ren, Y. Wang, F. Su, J.-X. Jiang, *J. Power Sources* **2016**, 317, 49.
- [56] J. K. Feng, Y. L. Cao, X. P. Ai, H. X. Yang, *J. Power Sources* **2008**, 177, 199.
- [57] Y. Gogotsi, R. M. Penner, *ACS Nano* **2018**, 12, 2081.
- [58] H. Lindström, S. Södergren, A. Solbrand, H. Rensmo, J. Hjelm, A. Hagfeldt, S.-E. Lindquist, *J. Phys. Chem. B* **1997**, 101, 7717.
- [59] V. Augustyn, E. R. White, J. Ko, G. Grüner, B. C. Regan, B. Dunn, *Mater. Horiz.* **2014**, 1, 219.
- [60] J.-D. Chai, M. Head-Gordon, *J. Chem. Phys.* **2008**, 128, 084106.
- [61] W. J. Hehre, R. Ditchfield, J. A. Pople, *J. Chem. Phys.* **1972**, 56, 2257.
- [62] M. M. Francl, W. J. Pietro, W. J. Hehre, J. S. Binkley, M. S. Gordon, D. J. DeFrees, J. A. Pople, *J. Chem. Phys.* **1982**, 77, 3654.
- [63] A. D. McLean, G. S. Chandler, *J. Chem. Phys.* **1980**, 72, 5639.
- [64] R. Krishnan, J. S. Binkley, R. Seeger, J. A. Pople, *J. Chem. Phys.* **1980**, 72, 650.
- [65] M. J. Frisch, J. A. Pople, J. S. Binkley, *J. Chem. Phys.* **1984**, 80, 3265.
- [66] S. I. Gorelsky, *AOMix: Program for Molecular Orbital Analysis* **2012**, <http://www.sg-chem.net/>.
- [67] S. I. Gorelsky, A. B. P. Lever, *J. Organomet. Chem.* **2001**, 635, 187.
- [68] T. Tao, H.-F. Qian, K. Zhang, J. Geng, W. Huang, *Tetrahedron* **2013**, 69, 7290.
- [69] F. Lombeck, D. Di, L. Yang, L. Meraldi, S. Athanasopoulos, D. Credgington, M. Sommer, R. H. Friend, *Macromolecules* **2016**, 49, 9382.
- [70] R. Steyrleuthner, Y. Zhang, L. Zhang, F. Krafft, B. P. Cherniawski, R. Bittl, A. L. Briseno, J.-L. Bredas, J. Behrends, *Phys. Chem. Chem. Phys.* **2017**, 19, 3627.
- [71] Z. Niu, H. Wu, L. Liu, G. Dai, S. Xiong, Y. Zhao, X. Zhang, *J. Mater. Chem. A* **2019**, 7, 10581.